

Upcycling the spent graphite/LiCoO₂ batteries for high-voltage graphite/LiCoPO₄-co-workable dual-ion batteries

Miao Du, Hongyan Lü, Kaidi Du, Shuohang Zheng, Xiaotong Wang, Xiaotong Deng, Ronghua Zeng, and Xinglong Wu

Cite this article as:

Miao Du, Hongyan Lü, Kaidi Du, Shuohang Zheng, Xiaotong Wang, Xiaotong Deng, Ronghua Zeng, and Xinglong Wu, Upcycling the spent graphite/LiCoO₂ batteries for high-voltage graphite/LiCoPO₄-co-workable dual-ion batteries, *Int. J. Miner. Metall. Mater.*, 31(2024), No. 7, pp. 1745-1751. <https://doi.org/10.1007/s12613-023-2807-2>

View the article online at [SpringerLink](#) or [IJMMM Webpage](#).

Articles you may be interested in

Liu-ye Sun, Bo-rui Liu, Tong Wu, Guan-ge Wang, Qing Huang, Yue-feng Su, and Feng Wu, [Hydrometallurgical recycling of valuable metals from spent lithium-ion batteries by reductive leaching with stannous chloride](#), *Int. J. Miner. Metall. Mater.*, 28(2021), No. 6, pp. 991-1000. <https://doi.org/10.1007/s12613-020-2115-z>

Cheng Yang, Jia-liang Zhang, Qian-kun Jing, Yu-bo Liu, Yong-qiang Chen, and Cheng-yan Wang, [Recovery and regeneration of LiFePO₄ from spent lithium-ion batteries via a novel pretreatment process](#), *Int. J. Miner. Metall. Mater.*, 28(2021), No. 9, pp. 1478-1487. <https://doi.org/10.1007/s12613-020-2137-6>

Hendrik Setiawan, Himawan Tri Bayu Murti Petrus, and Indra Perdana, [Reaction kinetics modeling for lithium and cobalt recovery from spent lithium-ion batteries using acetic acid](#), *Int. J. Miner. Metall. Mater.*, 26(2019), No. 1, pp. 98-107. <https://doi.org/10.1007/s12613-019-1713-0>

Qi Wang, Yue-yong Du, Yan-qing Lai, Fang-yang Liu, Liang-xing Jiang, and Ming Jia, [Three-dimensional antimony sulfide anode with carbon nanotube interphase modified for lithium-ion batteries](#), *Int. J. Miner. Metall. Mater.*, 28(2021), No. 10, pp. 1629-1635. <https://doi.org/10.1007/s12613-021-2249-7>

Toyohisa Fujita, Hao Chen, Kai-tuo Wang, Chun-lin He, You-bin Wang, Gjergj Dodbiba, and Yue-zhou Wei, [Reduction, reuse and recycle of spent Li-ion batteries for automobiles: A review](#), *Int. J. Miner. Metall. Mater.*, 28(2021), No. 2, pp. 179-192. <https://doi.org/10.1007/s12613-020-2127-8>

Qiao-kun Du, Qing-xia Wu, Hong-xun Wang, Xiang-juan Meng, Ze-kai Ji, Shu Zhao, Wei-wei Zhu, Chuang Liu, Min Ling, and Cheng-du Liang, [Carbon dot-modified silicon nanoparticles for lithium-ion batteries](#), *Int. J. Miner. Metall. Mater.*, 28(2021), No. 10, pp. 1603-1610. <https://doi.org/10.1007/s12613-020-2247-1>



IJMMM WeChat



QQ author group

Upcycling the spent graphite/LiCoO₂ batteries for high-voltage graphite/LiCoPO₄-co-workable dual-ion batteries

Miao Du¹, Hongyan Lü², Kaidi Du², Shuohang Zheng¹, Xiaotong Wang¹, Xiaotong Deng³, Ronghua Zeng³, and Xinglong Wu^{1,2}✉

1) Key Laboratory for UV Light-Emitting Materials and Technology of Ministry of Education, Northeast Normal University, Changchun 130024, China

2) Faculty of Chemistry, Northeast Normal University, Changchun 130024, China

3) School of Chemistry, South China Normal University, Guangzhou 510006, China

(Received: 18 October 2023; revised: 23 November 2023; accepted: 5 December 2023)

Abstract: The worldwide proliferation of portable electronics has resulted in a dramatic increase in the number of spent lithium-ion batteries (LIBs). However, traditional recycling methods still have limitations because of such huge amounts of spent LIBs. Therefore, we proposed an ecofriendly and sustainable double recycling strategy to concurrently reuse the cathode (LiCoO₂) and anode (graphite) materials of spent LIBs and recycled LiCoPO₄/graphite (RLCPG) in Li⁺/PF₆⁻ co-de/intercalation dual-ion batteries. The recycle-derived dual-ion batteries of Li/RLCPG show impressive electrochemical performance, with an appropriate discharge capacity of 86.2 mAh·g⁻¹ at 25 mA·g⁻¹ and 69% capacity retention after 400 cycles. Dual recycling of the cathode and anode from spent LIBs avoids wastage of resources and yields cathode materials with excellent performance, thereby offering an ecofriendly and sustainable way to design novel secondary batteries.

Keywords: recycle; lithium cobalt oxide; lithium cobalt phosphate; graphite; dual-ion batteries; spent lithium-ion batteries

1. Introduction

As one of the state-of-the-art methods, electrochemical energy storage technology for the transition from fossil energy to clean energy is in progress at an increasingly brisk pace, promoting the realization of a carbon-neutral future [1–4]. In particular, with outstanding electrochemical and good security performance, lithium-ion batteries (LIBs) have been widely used in power tools and portable electronics [5]. However, because the average lifespan of LIBs is only approximately five to eight years [6], ubiquitous electronic device consumption has rapidly increased spent batteries [7]. Compared with the 93800 t in 2019 [8–10], it is predicted that there will be approximately 11 Mt of spent LIBs by 2030. However, no more than 6wt% of spent LIBs are recycled worldwide, and there is still great room for improvement [11–12]. If the spent batteries are not disposed of properly, they will cause serious environmental pollution and waste of resources. The toxic substances (such as Co and V) in spent LIBs can also be hazardous to human health [13–14]. Moreover, considering the nonrenewable nature of valuable metals (e.g., Li, Co, and V), the effective recycling of spent LIBs, especially metallic resources, has become an urgent priority [15–16].

Common recycling methods are divided into destructive

decomposition and nondestructive recycling [17–18]. The destructive decomposition used for recycling valuable metals includes hydrometallurgy [19–23] and pyrometallurgy [24–26], which consumes high energy and many chemicals and produces a great deal of corrosive wastewater and waste gas [27]. In comparison, the nondestructive recycling (e.g., direct recycling [28–29] and upcycling [30–31]) of spent batteries is one of the best options owing to its nondestructive, inexpensive, and simple process [32–33]. Because direct recycling and upcycling have the advantages of process simplicity and enhanced functionality, respectively, some researchers directly recycled LiFePO₄ cathode materials to extract lithium from brine [8,27,34]. Yang *et al.* [35] and Du *et al.* [36] upcycled LiMn₂O₄ to the more stable and inexpensive LiFe_{0.6}Mn_{0.4}PO₄. Although the recycling ways of cathode and anode materials are comparatively mature, the incineration of spent materials will cause environmental pollution, especially for graphite (G) [37–38]. Therefore, dual recycling of the cathode and anode in spent LIBs can integrate into one new cathode as an efficient and novel strategy [8,39].

The widespread application of portable devices has generated enormous amounts of spent LiCoO₂ (LCO) and G, with active Li loss and irreversible phase transitions in LCO deteriorating electrochemical properties and increasing lattice spacing in G after long cycles [40–41]. The phosphate mater-

✉ Corresponding author: Xinglong Wu E-mail: xinglong@nenu.edu.cn

© University of Science and Technology Beijing 2024

ials have been extensively investigated because of the highly stable structural framework and excellent safety; however, the poor electrical conductivity hampers their electrochemical performance [42]. In this study, we propose an efficient and innovative strategy for the dual recycling of spent LCO cathode and G anode materials based on the research priority of high energy density and voltage combined with effectively handling the growing proportion of spent batteries [43]. To improve the poor electrical conductivity of LiCoPO_4 (LCP), we prepared a cation/anion-co-workable electrode (RLCPG) by mixing LCP and G with the mass ratio of 1:1. Reaction mechanism of dual-ion batteries (DIBs) is that LCP and G store Li^+ and PF_6^- , respectively. LCO powder was dissolved and supplemented with essential elements (Li , PO_4^{3-}) to prepare LCP, and the G powder restored the layer spacing after simple heat treatment. The prepared composite RLCPG material has high capacity, superior stability, and visibly improved stability. This closed-loop recycle approach exhibits a far-reaching significance for large-scale recycling of spent LIBs in the future, utilizes the main components of spent LIBs (cathode and anode), and contributes to new concepts for next-generation high-voltage LIBs.

2. Experimental

2.1. Recovery of spent LCO and G powder

Fig. 1 shows the recycling process of spent LCO batteries. First, pre-discharging the spent LCO batteries before manually dismantling prevents dangerous situations and allows more Li^+ to return to the cathode, which is conducive to

achieving a high recovery rate of Li. The spent LCO batteries were dismantled to obtain the cathode, anode, and separator. After scraping off from the cathode and anode plate, the LCO (Fig. S1) and G (Fig. S2) powder were washed and dried. The spent LCO powder after ball-milling (Fig. S3) was directly placed in the HNO_3 solution, and the reducing agent H_2O_2 was also added to promote the reduction of Co^{3+} . A certain amount of $\text{NH}_4\text{H}_2\text{PO}_4$ and LiNO_3 was added and stirred at 80°C to form a homogeneous gel. After drying and calcination, the regenerated LCP powder was obtained, and the spent G powder was calcined in an Ar atmosphere at 1300°C for 4 h. Finally, to improve the electronic conductivity of LCP, the LCP and G (RLCPG) materials were ground evenly in the mass ratio of 1:1 for the subsequent electrochemical test.

2.2. Material characterizations

The crystal structures of LCP, G, and RLCPG powder were tested by X-ray diffraction (XRD) on Rigaku D/MAX-2500. An inductively coupled plasma atomic emission spectrometer (ICP-AES) was employed to investigate the elemental content of LCP powder. Fourier-transform infrared spectroscopy (FTIR, Nicolet 6700) was applied to detect the chemical bond situation. Raman spectroscopy (HORIBA) was applied to characterize carbon composition. The valence states of C and Co were determined by X-ray photoelectron spectroscopy (XPS). The morphology and surface configuration were analyzed by scanning electron microscope (SEM) and transmission electron microscope (TEM).

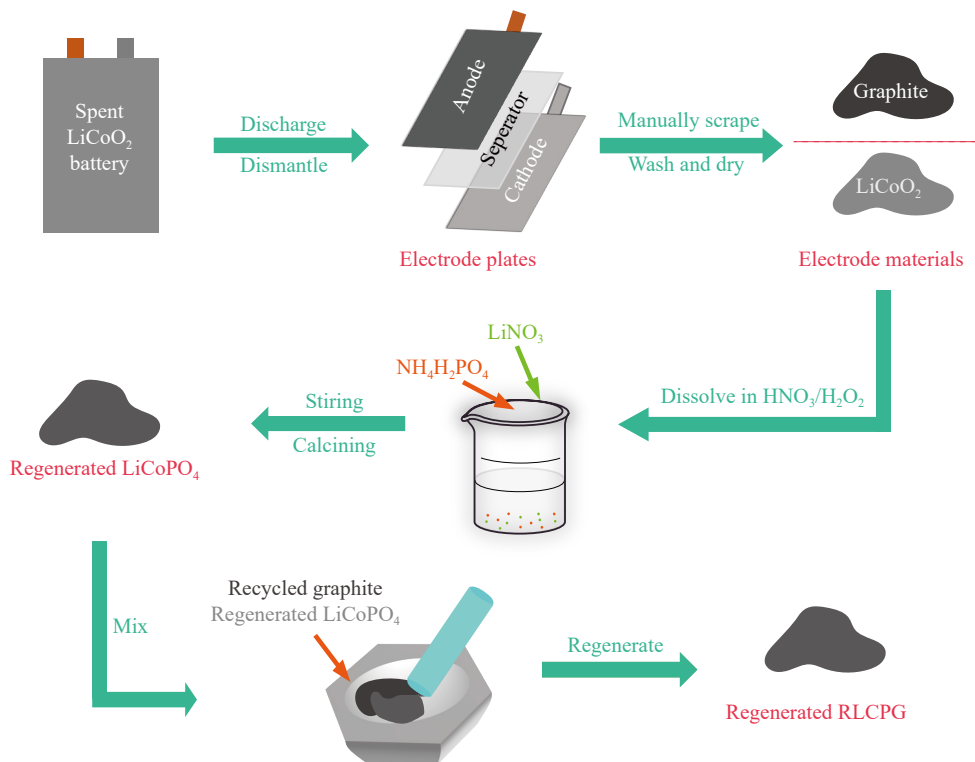


Fig. 1. Schematic of the recycling process for preparing a novel composite cathode material (RLCPG) via dual recycling of the cathode and anode of spent LiCoO_2 batteries.

2.3. Electrochemical measurements

All the electrochemical measurements of LCP, G, and RLCPG materials were performed by CR2032 stainless-steel coin cells in the potential range from 3.0 to 5.0 V vs. Li⁺/Li. The LCP, G, and RLCPG electrode, glass microfiber filter (Whatman), and Li foil were used as the cathode, separator, and anode in a half-cell. The electrolyte is 1 mol·L⁻¹ LiPF₆ dissolved in ethyl methyl carbonate. The three kinds of cathode were prepared by LCP, G, or RLCPG powder as active materials with acetylene black and polyvinylidene fluoride at the mass ratio of 8:1:1 into N-methyl-2-pyrrolidones and coated on Al foils. The galvanostatic charge/discharge (GCD) curves were conducted at various current densities (25, 50, 100, 200, 500, and 1000 mA·g⁻¹) using Neware. The cyclic voltammograms (CVs) were conducted on an electrochemical workstation (CHI660e). Electrochemical impedance spectroscopy (EIS, Princeton Applied Research P2000) in the 10 Hz to 1 MHz and galvanostatic intermittent titration technique (GITT, Arbin) tests at 3.0–5.0 V vs. Li⁺/Li were collected to study the LCP, G, and RLCPG electrode kinetics.

3. Results and discussion

3.1. Structure and morphology characterization

XRD was performed to study the crystal structure and phase purity. As shown in Fig. 2(a), the diffraction peaks of LCO and LCP coincided with the standard cards (PDF#89-6192 and PDF#70-2685), and there were no other obvious stray peaks. The results show that the LCP has an olivine crystal structure with a space group of *Pnma*. Fig. 2(b) shows the structure and purity characterization of the regenerated G, where all the diffraction peaks of the regenerated G corres-

pond to the standard card (PDF#89-8487). The peak (002) of XRD at 26.554° is significantly shifted to the right for the calcined treated G compared to the recycled untreated one, indicating that the layer spacing of the calcined G becomes smaller. This simple heat treatment can restore the layer spacing of spent G to an approximate initial level, which can increase the packing state and degree of order in G. Fig. 2(c) shows that the diffraction peaks of RLCPG are congruent with the standard cards of G and LCP, indicating that G and LCP coexist in RLCPG, and no other impurities appear with higher purity and more stable structure.

Fig. 2(d) shows the ratio between the different metals of the spent LCO batteries by ICP-AES, where the molar ratio of Li to Co is 0.884:1. Therefore, we added LiNO₃ in the follow-up experiment, and Li : Co is brought to 1.02:1. FTIR spectra (Fig. 2(e)) of RLCPG analyses the bonding and structural features, and it is obvious that the composite RLCPG contains characteristic peaks of G and LCP. Specifically, the Raman spectrum of RLCPG exhibits the characteristic peaks of P–O (1145–940 cm⁻¹), O–P–O (548 cm⁻¹), CoO₆ (515 and 580 cm⁻¹), and C=C (1653.35 cm⁻¹) [44]. Fig. 2(f) shows that the band belongs to the symmetric stretching of PO₄³⁻ (945 cm⁻¹). The two strong peaks (1350 and 1594 cm⁻¹) correspond to the D and G-band, and the intensity ratio (*I_D/I_G*) between them is 0.54, illustrating that the restored materials have a great graphitization degree [37].

The elemental composition of the RLCPG surface and the approximate valence composition can be monitored by XPS. Fig. 3(a) shows the full XPS spectrum of RLCPG, and it can be discerned that RLCPG comprises Li, Co, P, O, and C elements. Additionally, its Li (1s), Co (2p, 3p), P (2s, 2p), C (1s), and O (1s) peaks observed at their respective binding energy values are consistent with the reported values, indicating the effectiveness of the recovery method [45]. Fig. 3(b)

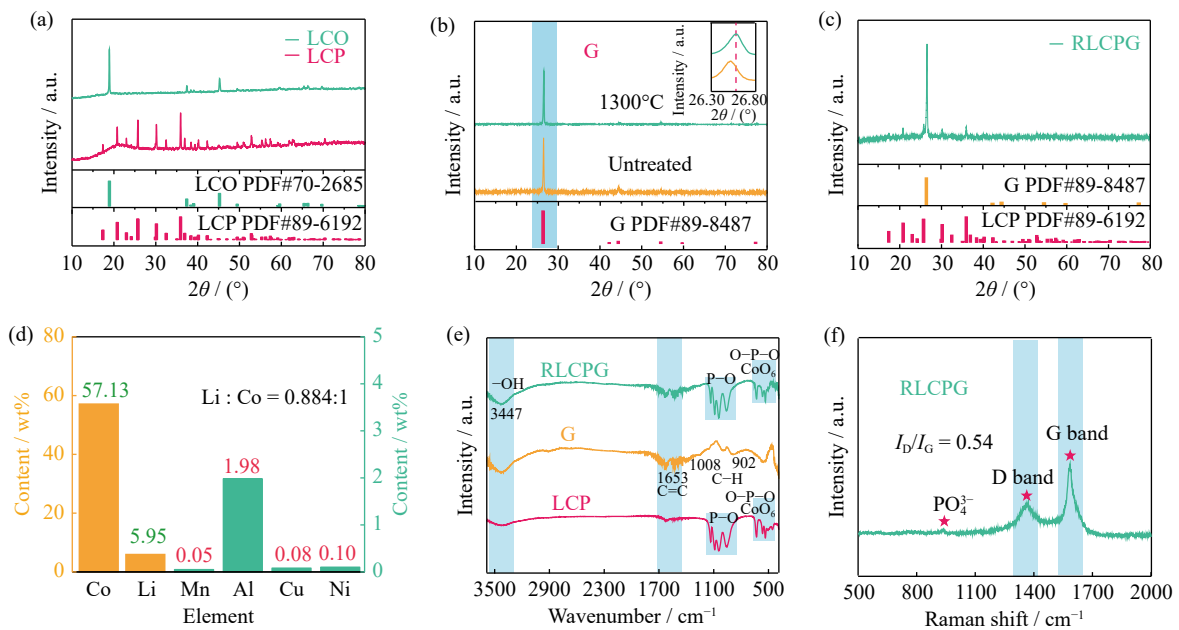


Fig. 2. Characterization results: X-ray diffraction pattern of (a) LiCoO₂ (LCO) and LiCoPO₄ (LCP), (b) graphite (G) (before and after calcination), and (c) recycled LiCoPO₄/graphite (RLCPG); (d) metal element (Co, Li, Mn, Al, Cu, and Ni) contents in spent LCO material; (e) Fourier-transform infrared spectroscopy spectra of RLCPG, G, and LCP; (f) Raman spectrum of RLCPG.

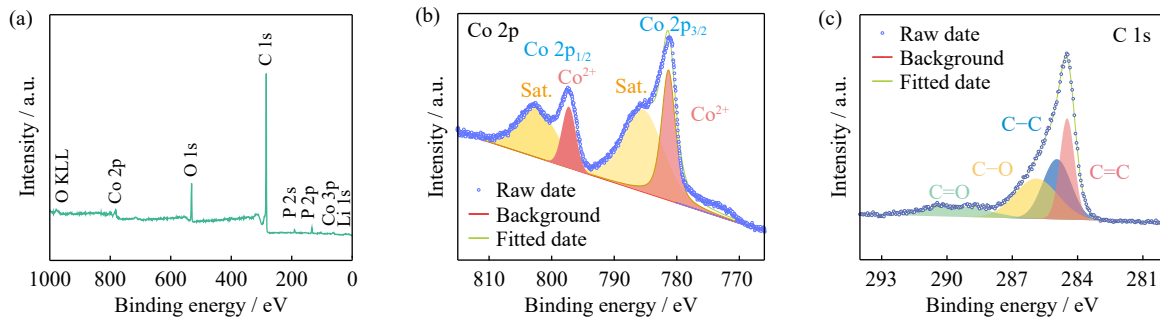


Fig. 3. (a) X-ray photoelectron spectroscopy (XPS) survey spectrum of recycled $\text{LiCoPO}_4/\text{graphite}$ (RLCPG); XPS spectra of (b) Co 2p and (c) C region of RLCPG.

shows the XPS spectrum of Co 2p of RLCPG. The Co 2p spectrum can be deconvoluted into two satellite peaks (785.34 and 802.24 eV), and two peaks at 797.24 and 781.32 eV correspond to Co^{2+} [46]. The XPS results show that Co in the recycled LCP was present in different valence states, which could be attributed to the disassembly of the spent LCO batteries still in a partially charged state. As shown in Fig. 3(c), the XPS of C 1s exhibits four characteristic peaks (C–O, C=C, C–C, and C=O) of G. These results provide further evidence that the composite material RLCPG is composed of G and LCP [47].

The particle size and morphological state of the RLCPG composites were observed by SEM (Fig. 4(a)). The particle size of LCP is nanometer and mainly ranges from 100 to 900 nm. The morphology of G is regular, indicating that heat treatment (1300°C for 5 h) improved the orderliness of G. It is evident from the image that LCP particles with smaller particle sizes are distributed near the larger-sized G and clustered together to form the RLCPG composite. TEM was

conducted to further investigate the microstructure of RLCPG (Fig. 4(b)). The G and LCP distribution pattern is consistent with the results of SEM tests. In the high-resolution TEM (HRTEM) image of the LCP (Fig. 4(c)), the clear lattice stripe spacing of 0.346 nm points to the (201) plane in the LCP lattice. Fig. 4(c) also shows the clear lattice fringes of the LCP, indicating its good crystallinity. The 0.336 nm crystal spacing in the HRTEM image of G (Fig. 4(d)) is consistent with the (002) crystal surface of G. As shown in Fig. 4(e), the energy-dispersive X-ray spectroscopy mapping demonstrates that all elements (Co, P, O, and C) are uniformly distributed in the RLCPG particles. A comparison of the mapping of carbon elements with the other three shows that G and LCP are distributed in a complementary manner. This further confirms that the LCP material is predominantly distributed near the bulk graphitic carbon material.

3.2. Electrochemical properties and diffusion kinetics

To assess the feasibility of RLCPG electrodes and invest-

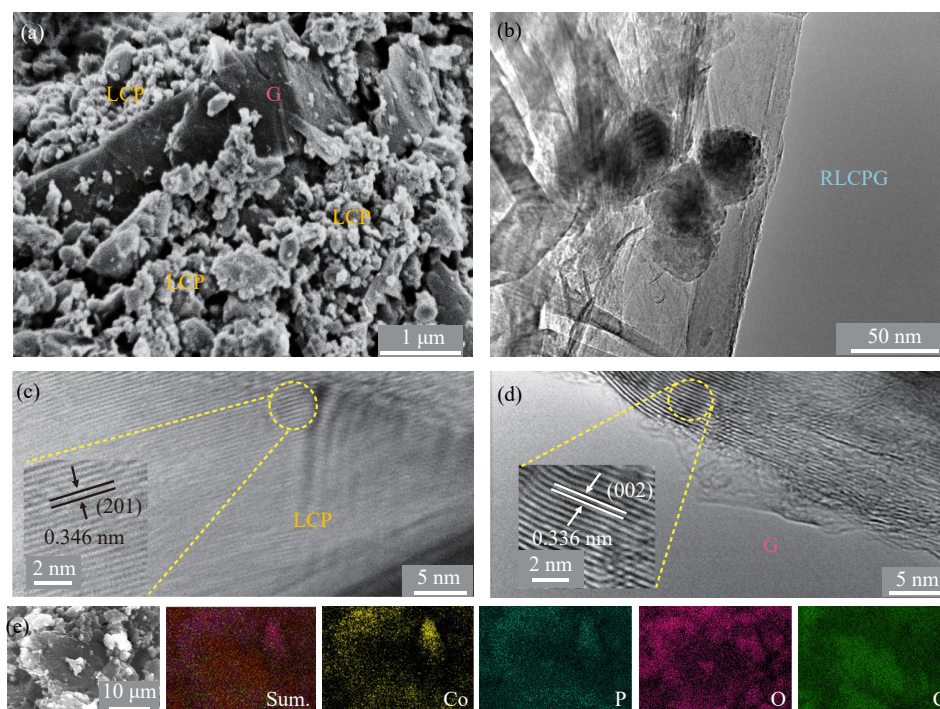


Fig. 4. Morphology and structure characterization of recycled $\text{LiCoPO}_4/\text{graphite}$ (RLCPG) powder: (a) scanning electron microscopy and (b) transmission electron microscopy images of RLCPG; high-resolution TEM images of (c) LCP and (d) G; (e) energy-dispersive X-ray elemental mappings (Co, P, O, and C) of RLCPG.

igate the deintercalation/intercalation process of Li⁺ and PF₆⁻ in RLCPG, we measured the electrochemical properties of the regenerated LCP, G, and RLCPG by Neware battery testing systems. As shown in Fig. 5(a), GCD tests (second cycle) were performed within a wide potential window of 3.0–5.0 V at 25 mA·g⁻¹. The regenerated LCP achieves a discharge-specific capacity of 74.7 mAh·g⁻¹ at 25 mA·g⁻¹. When G is the cathode, the discharge-specific capacity is approximately 86.9 mAh·g⁻¹. The charge/discharge potential plateau ranges from 4.0 to 5.0 V, suggesting that the PF₆⁻ in the electrolyte can also deintercalate/intercalate in G when used as the cathode in this potential range. Additionally, the RLCPG cathode achieves a higher capacity of 82.9 mAh·g⁻¹ than LCP, indicating PF₆⁻ storage between the interlayers of graphene sheets in G and confirming the feasibility of the DIB system based on the RLCPG electrode. It is satisfactory that RLCPG and LCP have comparable operating voltages (4.4 V), and the stability can also be greatly improved. Analogously, as shown in Fig. 5(b), three distinct oxidation and multiple relatively weaker reduction peaks appear on the CV curve of RLCPG, which are consistent with the potential plateau in the GCD test (Li⁺ deintercalation/intercalation from/into LCP and PF₆⁻ of electrolyte deintercalation/intercalation from/into G layers). Figs. S4 and S5 show the CV curves of LCP and G, respectively, which are consistent with Fig. 5(b). Therefore, the charge/discharge and CV curves of RLCPG are significantly different from those of LCP, indicating the presence of another ion co-de/intercalation other than Li⁺, i.e., PF₆⁻. The detailed schematic sketch (Fig. 5(c)) demonstrates the stepwise working mechanism of Li⁺ and PF₆⁻ in the composite RLCPG cathode. During the charging process, Li⁺ is

reversibly extracted from the RLCPG cathode and migrates to the Li anode via the electrolyte. In the high potential range of 4.0–5.0 V, the anion PF₆⁻ in the electrolyte is reversibly intercalated into the layered G to provide capacity by ion storage. The reverse process is achieved when discharging, thus creating a process in which anions/cations are jointly involved in the reaction.

Furthermore, the rate performance of LCP and RLCPG was evaluated in the potential window of 3.0–5.0 V. As shown in Figs. 5(d) and S6, composite RLCPG cathode displays the reversible capacities of 86.2, 76.3, 68.8, 62.6, 54.9, and 48.4 mAh·g⁻¹ at various current densities of 25, 50, 100, 200, 500, and 1000 mA·g⁻¹. Compared with LCP (83.4, 47.9, 29.5, 19.2, 11, and 6.5 mAh·g⁻¹), the RLCPG cathode shows a superior rate performance because of the good electrical conductivity of G. Fig. S7 demonstrates the rate performance of G. As in previous studies, the recycled G has appropriate performance, making it one of the best choices for DIBs. With the introduction of highly conductive material G in LCP, the rate performance of the composite RLCPG is greatly optimized, especially at the high current densities. Moreover, as we predicted, the composite RLCPG has more outstanding cycling stability (Fig. 5(e)). After 400 cycles, RLCPG still has 69% capacity retention, whereas LCP has only 15% at the current density of 25 mA·g⁻¹. The above electrochemical data demonstrate that dual recycling of cathode and anode from spent LIBs avoids resource wastage and yields cathode materials with excellent electrochemical performance.

Fig. 6(a) shows the electrochemical impedance spectroscopy (EIS) of the LCP and RLCPG. The EIS test was per-

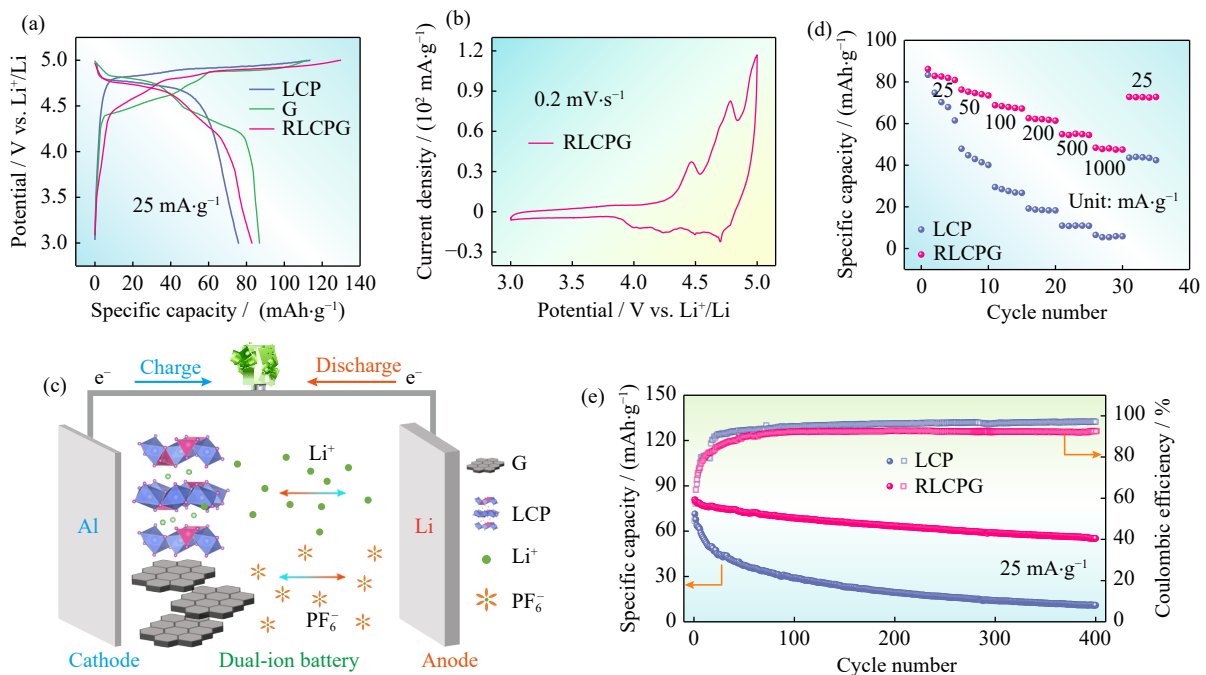


Fig. 5. Electrochemical performance: (a) galvanostatic charge/discharge curves (2nd cycle) of LiCoPO₄ (LCP), graphite (G), and recycled LiCoPO₄/graphite (RLCPG) at 25 mA·g⁻¹; (b) cyclic voltammogram profile of RLCPG at 0.2 mV·s⁻¹; (c) schematic of RLCPG//Li coin-type dual-ion batteries with stepwise Li⁺/PF₆⁻ deintercalation/intercalation; (d) rate capability at various current densities from 25 to 1000 mA·g⁻¹; (e) cycling performance of LCP and RLCPG at 25 mA·g⁻¹.

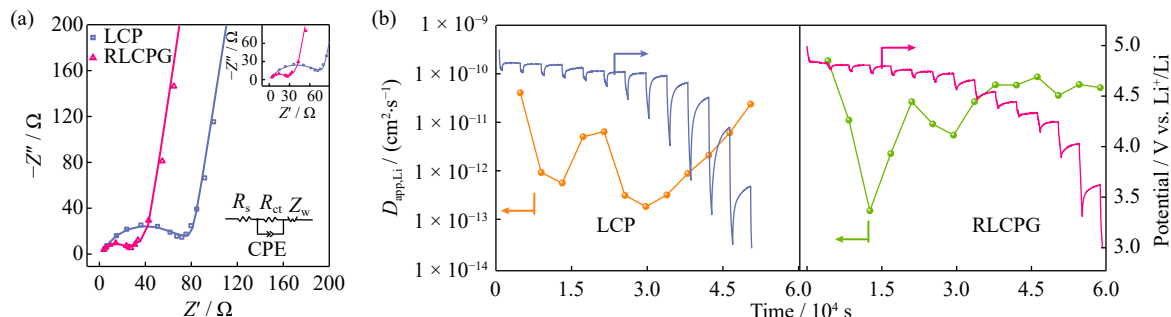


Fig. 6. Studies of LiCoPO_4 (LCP) and recycled LCP/graphite (RLCPG) electrode kinetics: (a) Nyquist plots of electrochemical impedance spectra and equivalent circuit (R_s , R_{ct} , Z_w , and CPE represent solution resistance, charge transfer resistance, Warburg impedance, and constant phase angle element); (b) galvanostatic intermittent titration technique tests and corresponding $D_{\text{app,Li}}$ of LCP and RLCPG electrode.

formed to determine the apparent diffusion ability of Li ions in the electrodes. The high-frequency region is associated with the charge transfer process. According to fitting the semicircle in the high-frequency region, the charge-transfer resistance (R_{ct}) of LCP is higher than that of RLCPG due to the sufficient electron-conducting channels of G. Similarly, the apparent Li-diffusion coefficient ($D_{\text{app,Li}}$) in the LCP and RLCPG electrode was compared by GITT test (Figs. 6(b) and S8). According to the GITT test, it is a 6 h relaxation after a pulse duration of 1 h at a current density of $5 \text{ mA}\cdot\text{g}^{-1}$. The diffusion coefficient of RLCPG was significantly higher than that of LCP. This is because the kinetics of RLCPG becomes faster after the proportional composite of LCP and G, and the transport ion motion of the cathode material is accelerated, thus affecting the change in the apparent ion diffusion coefficient.

4. Conclusion

In this study, we proposed an ecofriendly and sustainable double recycling strategy to concurrently reuse the spent cathode and anode materials of spent LIBs and innovatively used RLCPG in $\text{Li}^+/\text{PF}_6^-$ co-de/intercalation DIBs. The composite RLCPG cathode exhibited attractive stability and kinetics properties compared with LCP. At a current density of $25 \text{ mA}\cdot\text{g}^{-1}$, RLCPG displayed a discharge capacity of $86.2 \text{ mAh}\cdot\text{g}^{-1}$. Additionally, RLCPG demonstrated 69%, while LCP showed only 15% capacity retention after 400 cycles at a current of $25 \text{ mA}\cdot\text{g}^{-1}$. The apparent ion-diffusive coefficients of the LCP complexed with G were considerably enhanced, further indicating an improvement in the electrical conductivity of LCP. In contrast to the traditional recycling process, dual recycling of cathode and anode from spent LIBs avoids resource wastage and yields cathode materials with excellent performance.

Acknowledgements

This research was funded by the National Natural Science Foundation of China (No. 52173246) and the Science and Technology Planning Project of Guangzhou City, China (No. 2023B03J1278).

Conflict of Interest

Xinglong Wu is an editorial board member for this journal and was not involved in the editorial review or the decision to publish this article. All authors state that there is no conflict of interest.

Supplementary Information

The online version contains supplementary material available at <https://doi.org/10.1007/s12613-023-2807-2>.

References

- [1] P.K. Jones, U. Stimming, and A.A. Lee, Impedance-based forecasting of lithium-ion battery performance amid uneven usage, *Nat. Commun.*, 13(2022), No. 1, art. No. 4806.
- [2] Z.Y. Gu, J.Z. Guo, J.M. Cao, *et al.*, An advanced high-entropy fluorophosphate cathode for sodium-ion batteries with increased working voltage and energy density, *Adv. Mater.*, 34(2022), No. 14, art. No. 2110108.
- [3] Q.P. Lu, Z.H. Du, J. Wang, *et al.*, Editorial for special issue on renewable energy conversion, utilization and storage, *Int. J. Miner. Metall. Mater.*, 30(2023), No. 10, p. 1855.
- [4] Z.Z. Yu, G.Q. Zhao, F.L. Ji, *et al.*, Collaboratively enhancing electrochemical properties of $\text{LiNi}_{0.83}\text{Co}_{0.11}\text{Mn}_{0.06}\text{O}_2$ through doping and coating of quadrivalent elements, *Rare Met.*, 42(2023), No. 12, p. 4103.
- [5] R. Zhang, C.Y. Wang, P.C. Zou, *et al.*, Compositionally complex doping for zero-strain zero-cobalt layered cathodes, *Nature*, 610(2022), No. 7930, p. 67.
- [6] J. Lin, E.S. Fan, X.D. Zhang, *et al.*, Sustainable upcycling of spent lithium-ion batteries cathode materials: Stabilization by *in situ* Li/Mn disorder, *Adv. Energy Mater.*, 12(2022), No. 26, art. No. 2201174.
- [7] K. Kim, D. Raymond, R. Candeago, and X. Su, Selective cobalt and nickel electrodeposition for lithium-ion battery recycling through integrated electrolyte and interface control, *Nat. Commun.*, 12(2021), No. 1, art. No. 6554.
- [8] M. Du, J.Z. Guo, S.H. Zheng, *et al.*, Direct reuse of LiFePO_4 cathode materials from spent lithium-ion batteries: Extracting Li from brine, *Chin. Chem. Lett.*, 34(2023), No. 6, art. No. 107706.
- [9] K.Y. Zhang, Y.Z. Xu, Y.C. Lin, *et al.*, Enriching redox active sites by interconnected nanowalls-like nickel cobalt phosphosulfide nanosheets for high performance supercapacitors, *Chin. Chem. Lett.*, 32(2021), No. 11, p. 3553.
- [10] Y.T. Xu, S.J. Dai, X.F. Wang, X.W. Wu, Y.G. Guo, and X.X. Zeng, An ion-percolating electrolyte membrane for ultrahigh efficient and dendrite-free lithium metal batteries, *InfoMat*,

- 5(2023), No. 12, art. No. e12498.
- [11] J.J. Roy, S. Rarotra, V. Krikstolaityte, et al., Green recycling methods to treat lithium-ion batteries e-waste: A circular approach to sustainability, *Adv. Mater.*, 34(2022), No. 25, art. No. 2103346.
- [12] M. Xiang, W.X. Fan, W. Lin, et al., Triple kill: Fabrication of composites coming from waste face masks, polystyrene microplastics, graphene, and their electromagnetic interference shielding behaviors, *Carbon Neutralization*, 2(2023), No. 5, p. 616.
- [13] K.D. Du, E.H. Ang, X.L. Wu, and Y.C. Liu, Progresses in sustainable recycling technology of spent lithium-ion batteries, *Energy Environ. Mater.*, 5(2022), No. 4, p. 1012.
- [14] J. Wang, Y.F. Yuan, X.H. Rao, et al., Realizing high-performance Na₃V₂(PO₄)₂O₂F cathode for sodium-ion batteries via Nb-doping, *Int. J. Miner. Metall. Mater.*, 30(2023), No. 10, p. 1859.
- [15] Y.N. Yang, Y.J. Yang, C.L. He, et al., Solvent extraction and separation of cobalt from leachate of spent lithium-ion battery cathodes with N263 in nitrite media, *Int. J. Miner. Metall. Mater.*, 30(2023), No. 5, p. 897.
- [16] H.Y. Lu, R.L. Hou, S.Y. Chu, H.S. Zhou, and S.H. Guo, Progress on modification strategies of layered lithium-rich cathode materials for high energy lithium-ion batteries, *Acta Phys. Chim. Sin.*, 39(2023), No. 7, art. No. 2211057.
- [17] Z.J. Baum, R.E. Bird, X. Yu, and J. Ma, Lithium-ion battery recycling—Overview of techniques and trends, *ACS Energy Lett.*, 7(2022), No. 2, p. 712.
- [18] C.M. Costa, J.C. Barbosa, R. Gonçalves, H. Castro, F.J. del Campo, and S. Lanceros-Méndez, Recycling and environmental issues of lithium-ion batteries: Advances, challenges and opportunities, *Energy Storage Mater.*, 37(2021), p. 433.
- [19] M. Wasesa, T. Hidayat, D.T. Andariesta, et al., Economic and environmental assessments of an integrated lithium-ion battery waste recycling supply chain: A hybrid simulation approach, *J. Clean. Prod.*, 379(2022), art. No. 134625.
- [20] R.C. Xu, L.H. Jiang, N. Duan, et al., Research on microstructure of membrane-slime layer on lead-based anode surface in zinc hydrometallurgy by combining μ -XRF with mm-XRF, *J. Clean. Prod.*, 379(2022), art. No. 134568.
- [21] X.T. Wang, Z.Y. Gu, E.H. Ang, X.X. Zhao, X.L. Wu, and Y.C. Liu, Prospects for managing end-of-life lithium-ion batteries: Present and future, *Interdiscip. Mater.*, 1(2022), No. 3, p. 417.
- [22] T. Zhong, H.Y. Zhang, M.C. Song, et al., FeCoNiCrMo high entropy alloy nanosheets catalyzed magnesium hydride for solid-state hydrogen storage, *Int. J. Miner. Metall. Mater.*, 30(2023), No. 11, p. 2270.
- [23] Y.L. Heng, Z.Y. Gu, J.Z. Guo, and X.L. Wu, Research progresses on vanadium-based cathode materials for aqueous zinc-ion batteries, *Acta Phys. Chim. Sin.*, 37(2021), No. 3, art. No. 2005013.
- [24] L. Cassayre, B. Guzhov, M. Zielinski, and B. Biscans, Chemical processes for the recovery of valuable metals from spent nickel metal hydride batteries: A review, *Renewable Sustainable Energy Rev.*, 170(2022), art. No. 112983.
- [25] Y.H. Miao, S.Y. Qi, G. Chen, et al., Efficient removal of As, Cu and Cd and synthesis of photo-catalyst from Cu-smelting waste acid through sulfide precipitation by biogenic gaseous H₂S produced by anaerobic membrane bioreactor, *Chem. Eng. J.*, 451(2023), art. No. 138096.
- [26] H. Dang, Z.D. Chang, H.L. Zhou, S.H. Ma, M. Li, and J.L. Xiang, Extraction of lithium from the simulated pyrometallurgical slag of spent lithium-ion batteries by binary eutectic molten carbonates, *Int. J. Miner. Metall. Mater.*, 29(2022), No. 9, p.1715.
- [27] K.D. Du, Y.F. Meng, X.X. Zhao, et al., A unique co-recovery strategy of cathode and anode from spent LiFePO₄ battery, *Sci. China Mater.*, 65(2022), No. 3, p. 637.
- [28] J. Lin, J.W. Wu, E.S. Fan, et al., Environmental and economic assessment of structural repair technologies for spent lithium-ion battery cathode materials, *Int. J. Miner. Metall. Mater.*, 29(2022), No. 5, p. 942.
- [29] T. Wang, H.M. Luo, Y.C. Bai, J.L. Li, I. Belharouak, and S. Dai, Direct recycling of spent NCM cathodes through ionothermal lithiation, *Adv. Energy Mater.*, 10(2020), No. 30, art. No. 2001204.
- [30] B. Xu, P. Dong, J.G. Duan, D. Wang, X.S. Huang, and Y.J. Zhang, Regenerating the used LiFePO₄ to high performance cathode via mechanochemical activation assisted V⁵⁺ doping, *Ceram. Int.*, 45(2019), No. 9, p. 11792.
- [31] X.Q. Meng, H.B. Cao, J. Hao, P.G. Ning, G.J. Xu, and Z. Sun, Sustainable preparation of LiNi_{1/3}Co_{1/3}Mn_{1/3}O₂-V₂O₅ cathode materials by recycling waste materials of spent lithium-ion battery and vanadium-bearing slag, *ACS Sustainable Chem. Eng.*, 6(2018), No. 5, p. 5797.
- [32] S.H. Zheng, X.T. Wang, Z.Y. Gu, J.Z. Guo, X.L. Wu, and H.Y. Xu, Advances and challenges on recycling the electrode and electrolyte materials in spent lithium-ion batteries, *Mater. Lab.*, 1(2022), No. 4, art. No. 220036.
- [33] Z.Y. Gu, J.Z. Guo, X.X. Zhao, et al., High-ionicity fluorophosphate lattice via aliovalent substitution as advanced cathode materials in sodium-ion batteries, *InfoMat*, 3(2021), No. 6, p. 694.
- [34] M.C. Guo, W. Tang, Y. Hong, et al., Self-carbonization of soluble organic cathodes enables stable Na-ion batteries, *Sci. China Mater.*, 66(2023), No. 7, p. 2621.
- [35] Y. Yang, J.Z. Guo, Z.Y. Gu, et al., Effective recycling of the whole cathode in spent lithium ion batteries: From the widely used oxides to high-energy/stable phosphates, *ACS Sustainable Chem. Eng.*, 7(2019), No. 14, p. 12014.
- [36] M. Du, K.D. Du, J.Z. Guo, et al., Direct reuse of oxide scrap from retired lithium-ion batteries: Advanced cathode materials for sodium-ion batteries, *Rare Met.*, 42(2023), No. 5, p. 1603.
- [37] J.L. Yang, X.X. Zhao, W.H. Li, et al., Advanced cathode for dual-ion batteries: Waste-to-wealth reuse of spent graphite from lithium-ion batteries, *eScience*, 2(2022), No. 1, p. 95.
- [38] K.K. Jena, A. AlFantazi, and A.T. Mayyas, Efficient and cost-effective hybrid composite materials based on thermoplastic polymer and recycled graphite, *Chem. Eng. J.*, 430(2022), art. No. 132667.
- [39] Y.F. Meng, H.J. Liang, C.D. Zhao, et al., Concurrent recycling chemistry for cathode/anode in spent graphite/LiFePO₄ batteries: Designing a unique cation/anion-co-workable dual-ion battery, *J. Energy Chem.*, 64(2022), p. 166.
- [40] N.J. Zhang, W.J. Deng, Z.X. Xu, and X.L. Wang, Upcycling of spent LiCoO₂ cathodes via nickel- and manganese-doping, *Carbon Energy*, 5(2023), No. 1, art. No. e231.
- [41] J.X. Zhang, P.F. Wang, P.X. Bai, et al., Interfacial design for a 4.6 V high-voltage single-crystalline LiCoO₂ cathode, *Adv. Mater.*, 34(2022), No. 8, art. No. 2108353.
- [42] J.Z. Guo, H.X. Zhang, Z.Y. Gu, et al., Heterogeneous NASICON-type composite as low-cost, high-performance cathode for sodium-ion batteries, *Adv. Funct. Mater.*, 32(2022), No. 52, art. No. 2209482.
- [43] J.Y. Wu and C.J. Tsai, Qualitative modeling of the electrolyte oxidation in long-term cycling of LiCoPO₄ for high-voltage lithium-ion batteries, *Electrochim. Acta*, 368(2021), art. No. 137585.
- [44] N. Priyadharsini, S. Shanmugapriya, P.R. Kasturi, S. Surendran, and R.K. Selvan, Morphology-dependent electrochemical properties of sol-gel synthesized LiCoPO₄ for aqueous hybrid capacitors, *Electrochim. Acta*, 289(2018), p. 516.
- [45] Y. Wang, J.Y. Qiu, Z.B. Yu, et al., AlF₃-modified LiCoPO₄ for an advanced cathode towards high energy lithium-ion battery, *Ceram. Int.*, 44(2018), No. 2, p. 1312.
- [46] X.R. Yang, C.W. Wang, P.F. Yan, et al., Pushing lithium cobalt oxides to 4.7V by lattice-matched interfacial engineering, *Adv. Energy Mater.*, 12(2022), No. 23, art. No. 2200197.
- [47] H.J. Liang, Z.Y. Gu, X.X. Zhao, et al., Ether-based electrolyte chemistry towards high-voltage and long-life Na-ion full batteries, *Angew. Chem. Int. Ed.*, 60(2021), No. 51, p. 26837.